JJAP Series 4
Proc. of 1990 Intern. MicroProcess Conference pp. 52–57

Electron Beam Direct Writing Technologies for 0.3-μm ULSI Devices

Koichi MORIIZUMI, Susumu TAKEUCHI, Takeshi FUJINO,
Satoshi AOYAMA, Masahiro YONEDA, Hiroaki MORIMOTO
and Yaichiro WATAKABE

LSI R&D Laboratory, Mitsubishi Electric Corporation, 4-1 Mizuhara, Itami 664

(Received July 17, 1990; accepted for publication September 22, 1990)

Electron beam direct writing technologies for 0.3-μm devices are studied in this paper. In order to prevent charging effects, TQV, which is a varnish consisting of 7,7,8,8-tetracyano quino dimethane complex salt, has been coated on the top layer of a trilayer resist system. The effectiveness of TQV coating is indicated by the experimental results obtained from test patterns. A proximity effect correction system with several strategies to reduce the correction time and output data volume has been developed. These technologies have been adopted for the fabrication of ULSI circuit patterns with the dimension of about 0.3 μm. The calculation time and the output data volume of a proximity effect correction are reduced considerably by using new methods. It is revealed that 0.3-μm ULSI patterns can be precisely fabricated by these new technologies.

KEYWORDS: electron beam lithography, electron beam direct writing, ULSI, multilayer resist, charging, proximity effect, hierarchical data structure

§1. Introduction

Electron beam (EB) direct writing has been used to fabricate very fine devices such as 0.1–0.2 μm Si transistors,[1] GaAs devices,[2,3] Fresnel zone plates[4] and gratings. For such fabrications, its inherent high-resolution capability makes it the only lithography tool.[5] However, EB direct writing has not been applied to the development of ultralarge-scale integrated circuits (ULSI) which have a large amount of dense patterns with submicron dimensions because the throughput is substantially lower than that of optical lithography and the proximity effects must be corrected.

Recently, the throughput of EB direct writing has been improved by using a high throughput variable-shaped EB lithography system,[6] and a high-resolution, high-sensitivity resist.[7] A multilayer resist system has also been used to provide high resolution and durability to dry etching. However, a side effect of charging is caused when using the multilayer resist system. Furthermore, this phenomenon is amplified by using an EB writing system with high current density.

One of the most serious problems is the proximity effect. Many kinds of proximity effect correction methods have been developed.[8–10] Among them, the dose correction method is the most suitable because a variable-shaped EB system can easily modify dosage in every shot. Also, proximity effect correction methods to reduce the calculating time and output data volume have been studied[11] in order to accomplish the fabrication of ULSI devices using EB direct writing.

The aim of this paper is to describe the development of high accuracy EB direct writing technologies for fabricating 0.3-μm ULSI whose dimension exceeds the resolution limit of optical lithography. The key technologies for developing them, (1) reduction of EB charging in a multilayer resist and (2) a high-performance proximity effect correction system, will be presented.

§2. Process-Flow Overview

A trilayer resist system is adopted to provide high resolution and durability to dry etching. A normal bottomlayer resist and spin-on-glass (SOG) as an intermediatelayer are spin-coated with the thicknesses of 1.7 μm and 0.14 μm, respectively. A SAL-601ER7[7] of 0.5 μm thickness is used as a toplayer resist. Prebaking is performed for one minute at 85°C on a hot plate. The EB exposure is done on JBX-6AIII at 20 kV and with the current density of 0.6 A/cm^2. The sensitivity of a toplayer resist is 5.4 μC/cm^2 in the case of the above-mentioned trilayer resist system. After exposure, 2 minutes of postexposure baking (PEB) at 105°C is done to assist crosslinking of the resist resin. A toplayer resist is developed by tetramethylammoniumhydroxide of 2.38%, then SOG and the bottomlayer are dry etched.

§3. Prevention of Charging Effects

This multilayer resist system suffers from charging phenomena caused by EB irradiation because the injected electrons cannot be discharged easily from the resist materials. Hence the trajectories of incident electrons are influenced by electrostatic force. The displacement of the written patterns due to the charging occurs as shown in Fig. 1(a).

To prevent the charging phenomena, a conductive-layer coating between TQV which is the varnish consisting of 7,7,8,8-tetracyano quino dimethane complex salt on the surface of toplayer resist is investigated. In order to avoid the intermixing of TQV and SAL-601ER7, polyvinylalcohol (PVA) is used. The PVA is coated with the thickness of 0.2 μm onto SOG and is baked for 2 minutes at 70°C. Then, TQV of 0.13 μm thickness is coated and is baked for 2 minute at 70°C. After EB exposure, TQV is removed with methylisobutylketone (MIBK) and PVA is removed with water. To analyze the pattern displacement and quantitatively evaluate the

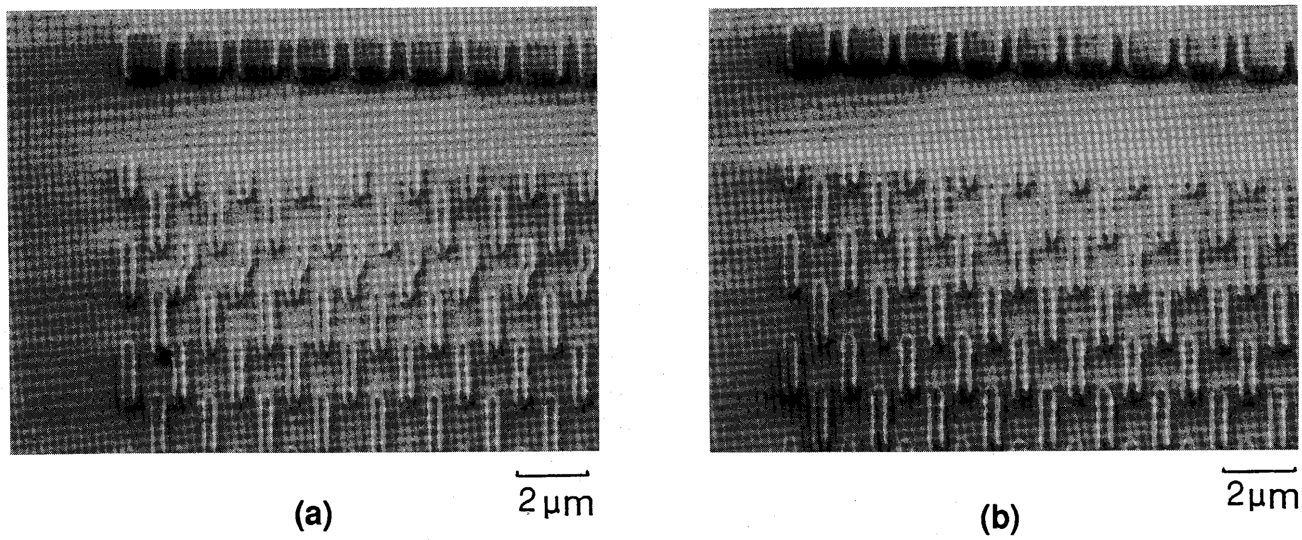

Fig. 1. SEM photographs of charging phenomena evaluation. Figure (a) is with conventional trilayer process, (b) is with TQV coating process.

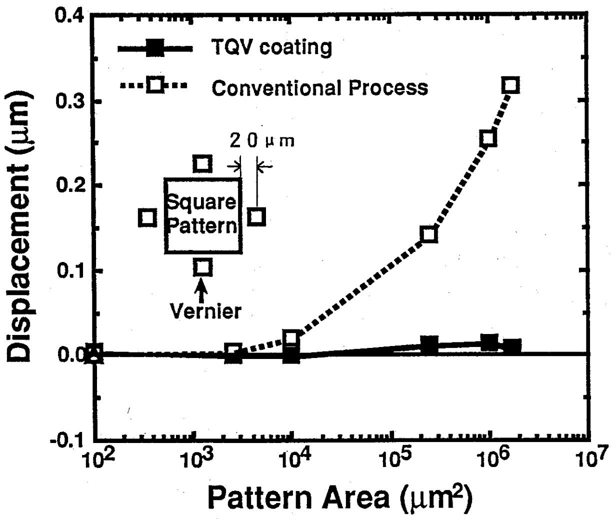

Fig. 2. Effectiveness of charging prevention processes. Pattern displacement is plotted vs large square pattern areas.

degree of charging reduction, test patterns consisting of verniers and large squares are designed. The distance between the center of verniers and the nearest side of a large square is fixed to 20 μm. Figure 2 shows the experimental results comparing the conventional process and the charging prevention process. This graph indicates that pattern displacement of over 0.3 μm occurs in the conventional trilayer process, and that the displacement is less in the new process. From these results, it is found that the TQV coating is very effective for reducing EB charging. The result using the test pattern with the TQV coating is shown in Fig. 1(b). It is revealed that the pattern displacement is eliminated in this new process.

§4. Proximity Effect Correction

A proximity effect correction system in practical use should have sufficient accuracy, reasonable throughput and small output data volume. In order to satisfy the above conditions simultaneously, the following strategies have been implemented.

(1) Basic algorithm with high performance and flexibility.

(2) Utilizing a table of energy intensity distribution (EID) where the definite integral values of Gaussian function are stored.

(3) Database with bucketing method for figure search.

(4) Utilizing the hierarchical data structure.

(5) Divide figures into a contour part and a kernel part, and partition the contour part into small elements.

(6) Reconnect the partitioned elements with the same correction dosage.

(7) Reconstruct figure arrays.

4.1 *Basic algorithm*

The proximity effect correction here utilizes the basic algorithm in which the dosage of each figure is determined to make the deposited energy at each edge of figures an equal dosage with an iterative calculation method. This algorithm is based on the assumption that the uniformity of the deposited energy at the edges mainly determines the pattern accuracy, and the deposited energy inside the figures does not have to be considered carefully. This algorithm can realize higher throughput than that which deals with both the edge and the inner part of figures precisely.

The EID function represented by the sum of two Gaussian distributions is used to calculate the deposited energy. The parameters of the EID function are calculated using Monte Carlo simulation and are verified by experiments.

4.2 *EID table*

To obtain the deposited energy at sample points, the definite integral of the Gaussian function must be calculated. It takes a long time to calculate these values. In this system, the 'EID table', in which the integral values are stored, is prepared prior to the proximity effect correction. The calculation time of the proximity correction is greatly reduced by referring to the integral values of the Gaussian function stored in the EID table.

4.3 *Database for figure search*

In order to calculate the deposited energy at a sample point, it is required to search for proximate figures which cause an effect on the point. The throughput of the figure search is an important concern in the case of correcting ULSI with a large amount of figures. In this system, the database of figures with a bucketing method is used to minimize the time for the figure search.

The schematic diagram of the database is shown in Fig. 3. The chip area is divided into buckets with the size of about 3 × (backscattering radius). Data buffers to store the address of figure data are allocated for each bucket. If a part of the figure is inside the bucket, the address of the figure is stored in the allocated buffer. An example is shown in Fig. 3. Figure A lies on bucket(2, 3) and bucket(3, 3), so the address of figure A is stored in the buffers of bucket(2, 3) and bucket(3, 3).

The procedure of figure search is as follows. At first, the bucket including a certain sample point is found. The figures stored in the buffers of this bucket and the surrounding 8 buckets are regarded as the proximate figures which have a possibility to influence the sample point. In the case of Fig. 3, the figures in bucket (i, j) $(i=2, 3, 4;$ $j=2, 3, 4)$ have the possibility to cause an effect on the sample point which is set on the upper side of figure A. The figures can be searched rapidly using the address of figure data stored in the buffers.

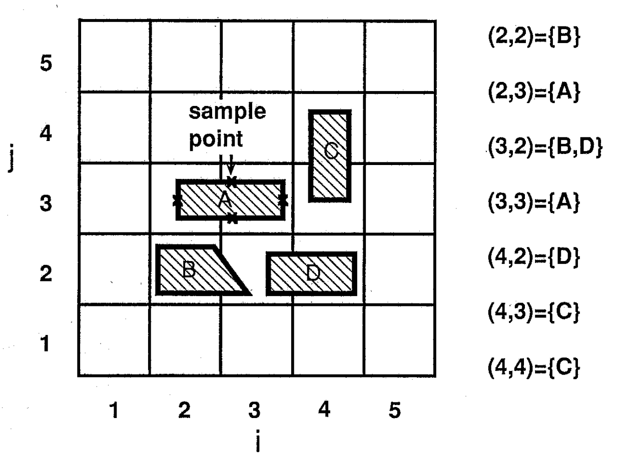

Fig. 3. Database for figure search. Each bucket is shown as (i, j). The size of a bucket is 3 × (backscattering radius). "$(i, j)=\{A\}$" means that the address of figure A is stored in the buffer of bucket (i, j).

4.4 *Hierarchical data structure*

Figure 4 shows the correction method utilizing the hierarchical data structure which consists of '*unit*' and '*area*'. '*Unit*' is a group of several figures like the concept of a '*cell*' used in the CAD database. '*Area*' means the territory in which the specific '*unit*' is placed as an array.

This method is described as follows.

(1) Construct '*unit*' and '*area*' (Fig. 4(a)).

The '*unit*' and '*area*' can be constructed automatically from the flattype of figure database.[12]

(2) Redefine '*area*' where the correction dosage of each '*unit*' is the same (Fig. 4(b)).

This '*area*' should be set as large as possible because the size of the '*area*' has a great influence on the throughput.

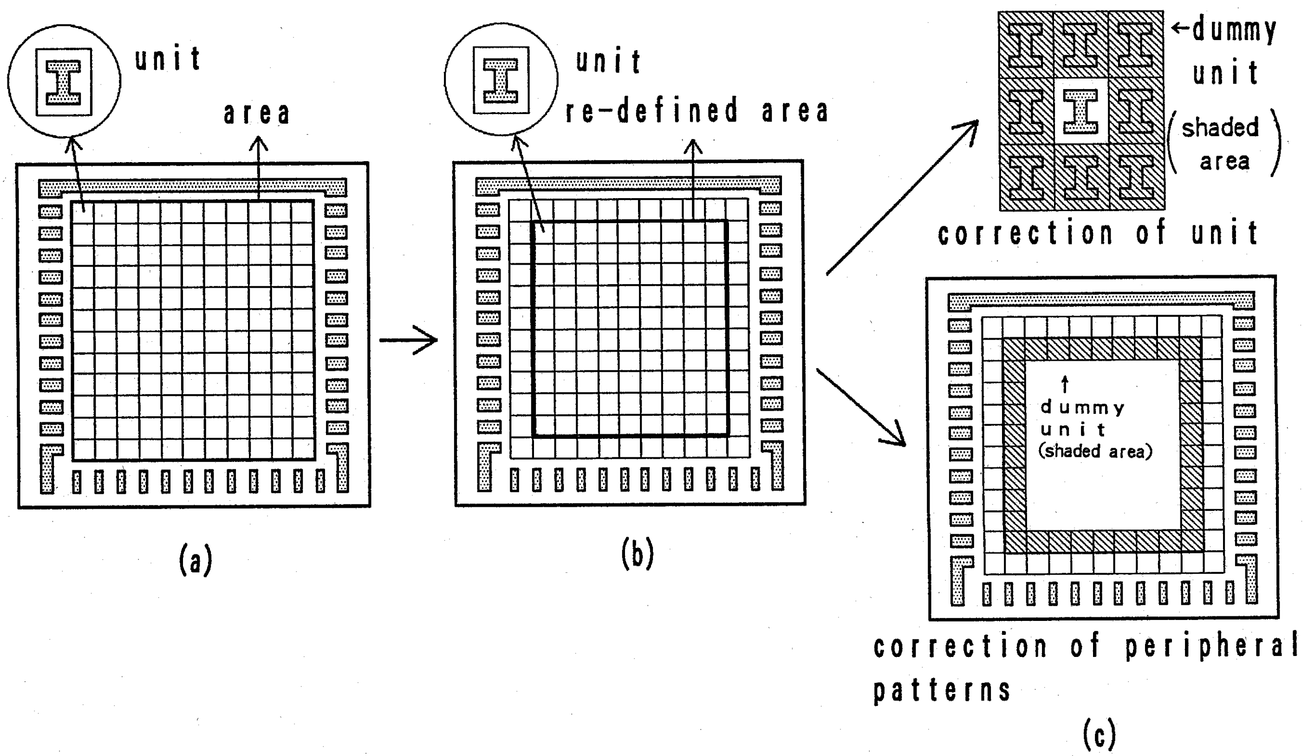

Fig. 4. Processing method utilizing hierarchical data structure.

The size of the '*area*' is decided by the preliminary evaluation with a test pattern.

(3) Perform the proximity effect correction to '*unit*' and the peripheral figures independently. The interaction between '*unit*' and the peripheral figures is taken into consideration using '*dummy units*' (Fig. 4(c)).

(4) Merge '*units*' and the peripheral figures after removing the '*dummy units*'.

This method is effective for memory devices to which a few kinds of '*units*' are referred at a great number of times. The required time to correct a large amount of figures in the '*area*' is only the time to correct several figures in '*unit*' and '*dummy units*'. This time is negligible compared with the required time to correct peripheral figures outside '*area*'. Therefore, the correction time can be reduced greatly with this method. The output data volume can also be reduced because many figures in the '*area*' are represented by a few kinds of '*units*' and '*area*'.

4.5 *Divide and reconnect figures*

The divide and reconnect method is shown in Fig. 5. The input figures of large size are divided into a contour part and a kernel part. The contour parts are partitioned into small elements. The accuracy of the proximity effect correction strongly depends on the size of the elements. As the element size becomes smaller, the correction accuracy becomes higher, but the calculation time becomes longer. Thus, an element size is determined considering the required accuracy and throughput. The appropriate constant dosage is assigned to the kernel part because the kernel part does not influence the accuracy significantly. The proximity effect correction is performed on all contour elements using the above described basic algorithm.

After the correction, as many elements as possible with the same dosage are connected. This function is indispensable to prevent the explosion of the output data amount.

4.6 *Reconstruct figure arrays*

The ULSI contains many figure arrays. After the above procedure, figure arrays are reconstructed by extracting the figures with the same shape and dosage in order to reduce the output data volume.

4.7 *Throughput and accuracy*

The basic throughput of the proximity correction system is evaluated using test patterns consisting of a matrix (100 × 100) of isolated squares. It is assumed that isolated squares are not divided into small elements. The width of the squares is equal to the distance between squares. The figure density is varied by changing the width of squares and the distance between squares from 0.2 μm to 1.0 μm. Figure 6 shows the basic throughput. A minicomputer with the capability of 6 million instructions per second (MIPS) was used. It is shown that the basic throughput, which is represented by the calculation time per one figure, depends on the figure density.

The accuracy is shown in Fig. 7. The pattern width of two extreme cases was measured by the EB metrology system. Without the correction, the width of isolated lines is smaller than the designed size, and the pattern linearity is not acceptable for a 0.3-μm ULSI. With the correction, it can be seen that good width agreement for an isolated line and a line between large pads is achieved. Figure 8 shows SEM photographs of the resist patterns without (a) and with (b) the proximity effect correction. Resist bridges between patterns are found in the case without the proximity effect correction. On the contrary, patterns are fabricated precisely with the proximity effect correction.

§5. Application to 0.3-μm ULSI

The EB direct writing technologies described above have been applied to the prototyping of a dynamic ran-

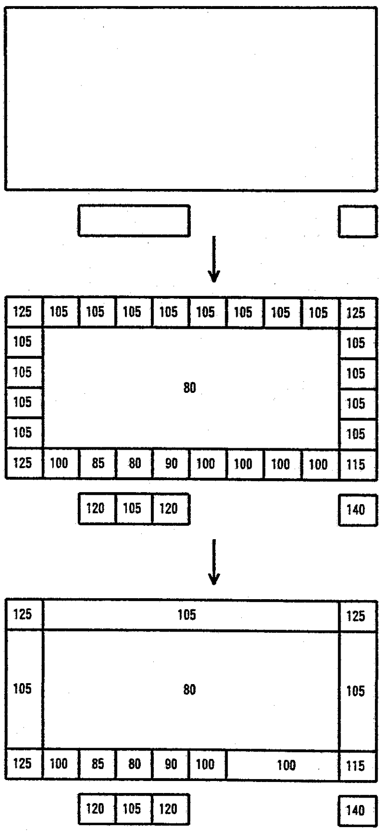

Fig. 5. Pattern division and reconnection methods. The number in figures indicates the relative dosage.

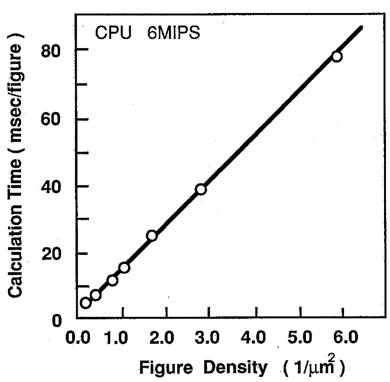

Fig. 6. Basic performance of proximity effect correction system.

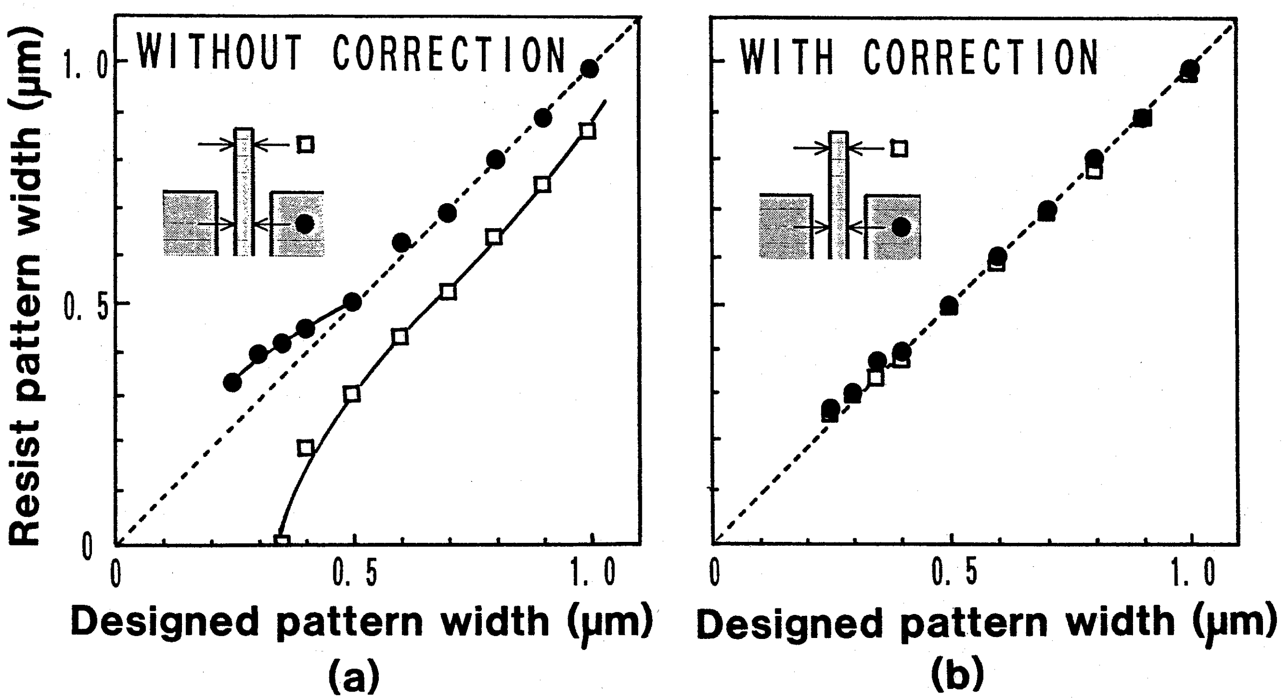

Fig. 7. SEM photographs of 0.3 μm test patterns for evaluating the accuracy of a proximity effect correction. (a) is without correction and (b) is with correction.

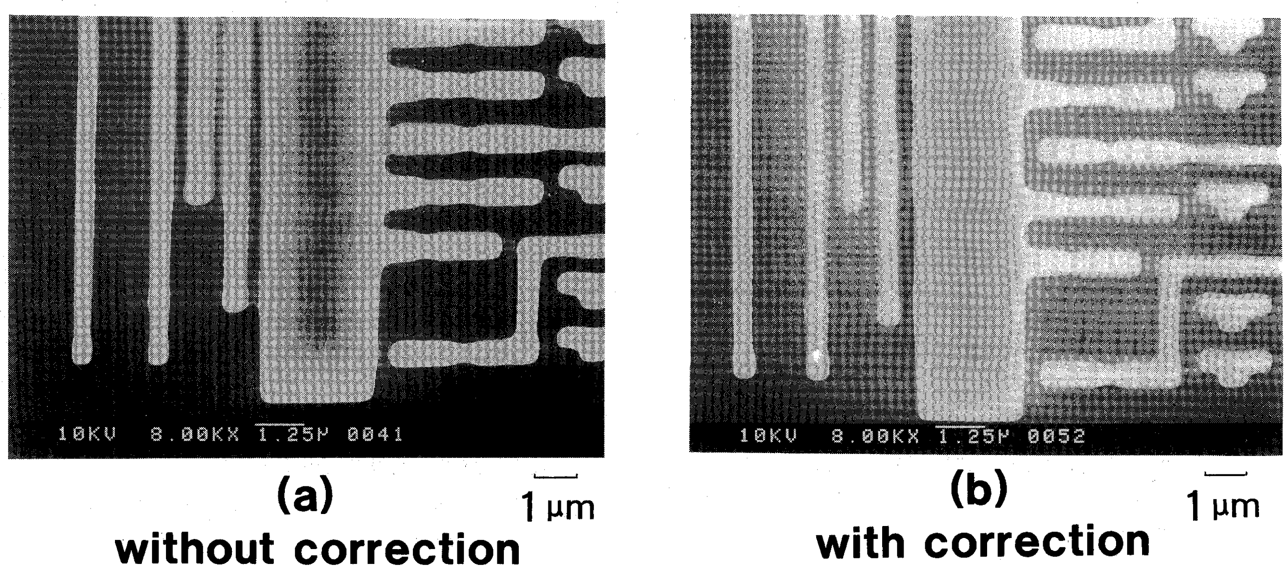

Fig. 8. Evaluation of patterns with 0.3 μm line. (a) SEM photograph without proximity correction, (b) SEM with proximity correction. Trilayer resist system was used.

dom access memory (DRAM) with 0.3-μm design rule. Typical DRAM layers, such as isolation, a transfer gate and others are processed with the EB direct writing. The specification regarding the figure count is indicated in Table I. This test pattern includes 1 Mbit memory cells.

The effectiveness of new features, such as utilizing a hierarchical data structure, reconnecting elements and reconstructing figure arrays, is shown in Figs. 9 and 10. In both the new and the conventional methods, the basic methods such as the basic correction algorithm, EID

Table I. Specification of 0.3 μm ULSI test pattern.

Layer	A	B	C
Figure count in a '*unit*'	6	8	24
Figure count in '*area*' (all units are expanded)	6.8 ($\times 10^5$)	9.1	27.2
Figure count in peripheral area	2.6 ($\times 10^5$)	2.3	7.1
Total figure count	9.4 ($\times 10^5$)	11.4	34.3
Rate (peripheral/total)	0.28	0.20	0.21

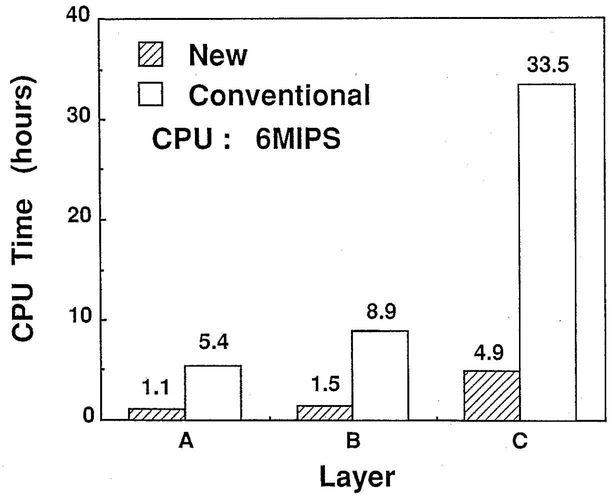

Fig. 9. Throughput improvement of proximity effect correction.

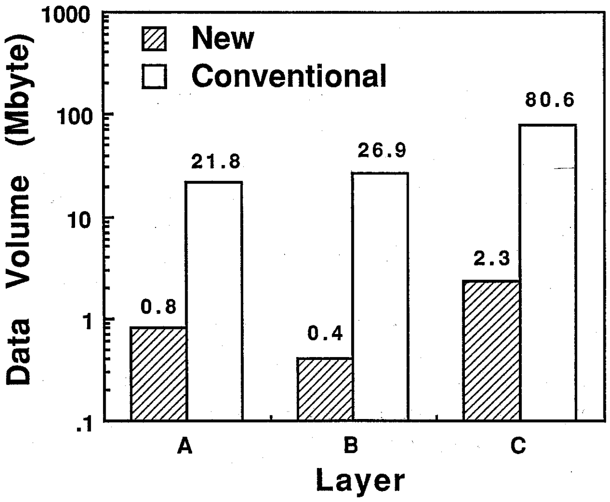

Fig. 10. Data volume reduction rate utilizing the new proximity correction system.

table, and the database using bucketing method are commonly used. The hierarchical data structure, reconnecting elements, and reconstructing figure arrays are not utilized in the conventional method. The correction time has been reduced to about 1/5–1/7 and the data volume has been compacted to 1/30–1/70. It is found that these methods are very effective for ULSI with a large amount of dense figures.

Figure 11 shows SEM photographs of the transfer gate layer of 0.3-μm-rule DRAM just after the bottom resist was etched. The high density of 0.3-μm patterns can be fabricated with high fidelity to the designed patterns.

§6. Conclusions

The EB direct writing technologies for fabricating 0.3-μm ULSI circuits have been developed. It has been in-

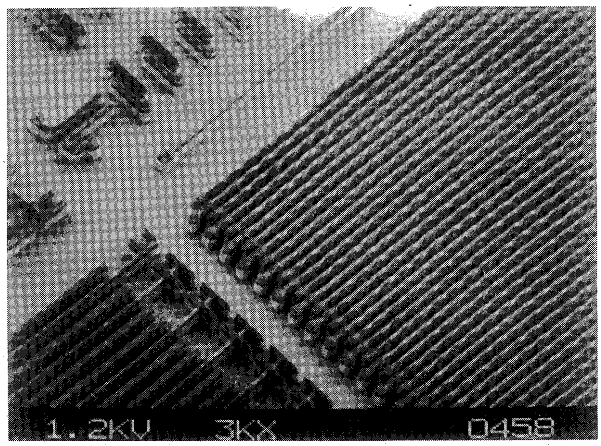

Fig. 11. SEM photograph of 0.3-μm ULSI pattern just after a bottom resist was dry etched.

dicated that the conductive-layer coating on a toplayer resist is effective for charging prevention. The proximity effect correction system, which has numerous advantages for high throughput, accuracy and small output data volume, has been developed. The newly developed EB writing technologies have been applied to fabricate a 0.3-μm ULSI with dense patterns. The correction time and output data volume have been reduced considerably. The high density of the 0.3-μm pattern has proven to be possible to fabricate with high design fidelity.

Acknowledgment

The authors are greatly thankful to Dr. H. Komiya and Dr. N. Abe for their encouragement during this study, and are also grateful to Nitto Chemical Industry Co. Ltd. for providing the TQV samples.

References

1) D. P. Kern, S. A. Rishton, T. H. P. Chang, G. A. Sai-Halasz, M. R. Wordman and E. Ganin: J. Vac. Sci. Technol. **B6**(6) (Nov/Dec 1988) 1836.
2) D. M. Tennant, S. C. Shunk, M. D. Feuer, J. M. Kuo, B. Tell, R. E. Behringer and T. Y. Chang: J. Vac. Sci Technol. **B6**(6) (Nov/Dec 1988) 1820.
3) D. J. Resnik, F. Ren, D. M. Tennant and R. F. Kopf: *Proc. SPIE* **1089** (1989) 103.
4) P. Unger, V. Bogl, H. Beneking, B. Niemann and P. Gurtmann: J. Vac. Sci. Technol. **B6**(1) (Jan/Feb 1988) 323.
5) A. N. Broers: Proc. Int. Symp. Micro Process 89, Kobe, 1989, Jpn. J. Appl. Phy. Series **3** (1989) 43.
6) A. Gonzales: *Proc. SPIE* **1089** (1989) 374.
7) M. deGrandpre, K. Graziano and S. D. Thompson: *Proc. SPIE* **923** (1988) 158.
8) M. Parikh: J. Appl. Phys. **50**(6) (Jun 1979).
9) G. Owen and P. Rissman: J. Appl. Phys. **54** (1983) 3573.
10) M. E. Haslam, J. F. McDonald, D. C. King, M. Bougeois, D. G. L. Chow and A. J. Steckl: J. Vac. Sci. Technol. **B3**(1) (Jan/Feb 1985) 165.
11) T. Abe, N. Ikeda, H. Kusakabe, R. Yoshikawa and T. Takigawa: J. Vac. Sci. Technol. **B7**(6) (Nov/Dec 1989) 1524.
12) K. Moriizumi, S. Takeuchi, K. Hosono, S. Matsuda, M. Yoshida, A. Shigetomi, Y. Watakabe and T. Kato: *Proc. SPIE* **1089** (1989) 93.